

# Long-time joint spectra and entanglement of two photoelectrons originating in interacting auto-ionization systems

**Jan Peřina Jr.**

Institute of Physics of Academy of Science of the Czech Republic, Joint Laboratory of Optics, 17. listopadu 50a, 772 07 Olomouc, Czech Republic  
E-mail: jan.perina.jr@upol.cz

**Antonín Lukš**

Palacký University, RCPTM, Joint Laboratory of Optics, 17. listopadu 12, 771 46 Olomouc, Czech Republic

**Wiesław Leoński**

Quantum Optics and Engineering Division, Institute of Physics, University of Zielona Góra, Prof. Z. Szafrana 4a, 65-516 Zielona Góra, Poland

**Abstract.** Two auto-ionization systems in a stationary optical field mutually interacting via the dipole-dipole interaction are considered. Their evolution is analytically found. Joint spectra of two ionized electrons are analyzed in detail in the long-time limit for comparable strengths of direct and indirect ionization paths as well as the dominating indirect ionization path. Entanglement in the state of two ionized electrons is quantified using the density of quadratic negativity. Suitable conditions for obtaining highly entangled states are discussed.

PACS numbers: 33.80.Eh,34.20.-b,03.65.Ud,32.80.-t

*Keywords:* two-electron ionization spectra, auto-ionization, dipole-dipole interaction, Fano model, bipartite entanglement, quadratic negativity

## 1. Introduction

Ionization is one of the most interesting physical processes arising from the interaction of atoms or molecules with electromagnetic fields. Ionized electrons are characterized by their ionization spectra that contain information about the electronic structure of the ionized atoms or molecules. For this reason, ionization processes have been used as a strong tool for the investigation of electronic structures [1, 2]. The ionization spectra are strongly sensitive to individual bound excited electronic states through which the ionization can efficiently proceed (for an extended list of references, see e.g. [3, 4, 5, 6]).

The mechanism of auto-ionization occurring with the contribution of a bound excited state has been extensively studied for He atoms containing only two electrons. Quantum mechanical calculations have shown that there is a large probability of exciting both electrons together [7] due to the strong electron-electron correlations present in the electronic ground state [8]. Energy of one of the excited electrons given to the other excited electron then allows ionization of this electron. The first electron returns to its ground state. This process modelled in [9, 10, 11] with the inclusion of an additional probe field has recently been observed using attosecond pump-probe spectroscopic techniques [12, 13].

The presence of an auto-ionizing state in atoms manifests itself in the ionization spectra by the so-called Fano zero [14]. It denotes an electron energy missing in the ionization spectrum. This occurs due to the completely destructive interference between different paths of ionization, including the interference between direct and indirect (through an auto-ionizing state) ionization processes [15]. This interference also results in sharp peaks in the ionization spectra caused by intense laser pulses [16, 17]. As predicted by Fano [14],  $n$  zeroes will be present for  $n$  auto-ionizing levels for an atom as long as only a single ionization channel is available. They are replaced by local minima when more ionization channels are present, and they may even disappear in molecules because of the presence of nuclear motion [18].

The presence of auto-ionizing states influences considerably many physical effects. For example, auto-ionization systems have been investigated as media exhibiting electromagnetically-induced transparency [19, 20, 21]. They have also been applied for slowing

down the light propagating through the medium with auto-ionizing states [20]. Moreover, special attention has been devoted to the problem of near-threshold ionization [22] including quantum anti-Zeno effect [23]. The role of elastic collisions and finite laser spectral width has been analyzed for such systems in [24]. Auto-ionization has even been considered for weak quantum fields [25], in particular, for squeezed light [26]. Interestingly, Fano profiles and Fano resonances can appear not only in typical atomic/optical models. They have been found, for instance, in plasmonic systems [27, 28], various nanoscale structures [29] including quantum dots [30] or in a broad range of superconducting systems [31, 32, 33]. We note that states of the continuum and bound states participate together in the effect called the Feshbach resonance [34]. In this effect, a quasi-bound molecular state is formed from the state of two free atoms. This results in considerable enhancement of inelastic collision processes [35].

Ionization can also be observed due to the electronic Coulomb interaction between two excited electrons being at two neighbor atoms. In this case, energy of one excited electron is given to the excited electron on the neighbor atom at which ionization occurs [36]. If two excited electrons emerge from the interaction with the strong electromagnetic field, we have two-center resonant photo-ionization [37, 38]. Also two-center dielectronic recombination [39, 38] which is just the inverse process in which a free electron is captured by a positively charged system of two neighbor atoms has been suggested. These effects are important in atomic and molecular clusters in which the exponential character of these processes can be modified by additional interactions, e.g. by capturing the ionized electron [40].

In an intense external field, double ionization may occur leaving two free ionized electrons [7]. It has been extensively studied in isolated atoms or molecules [41]. The dynamics of double ionization is predominantly governed by the strong Coulomb interaction among the electrons and the core of an atom. As a consequence, strong correlations in momenta of two ionized electrons occur [42, 43]. Considering He atoms, rotational and bending modes of the two-excited-electron motion preceded the ionization have been identified [44]. Double ionization of Ne atoms has been experimentally studied in [45].

Here, we consider another process in which

two electrons are ionized in such a way that their energies are highly correlated. Contrary to the double ionization model of a single atom, we consider a system of two neighbor atoms or molecules under the interaction with a strong cw external field. Each atom or molecule provides one ionized electron. We assume here that each atom or molecule can be ionized through an auto-ionizing level or by the process of direct ionization. We show that, as a result of the dipole-dipole interaction between two atoms or molecules, the state of two ionized electrons can be strongly entangled and both electrons can exhibit strong spectral correlations.

The model considered here is analyzed using the algebraic method applied already by Fano [14]. Our model represents a generalization of the previously developed models in which ionization spectra and correlations between an ionized electron and a bound electron found at a neighbor atom have been studied. It has been shown that the so-called dynamical Fano zeroes occurring once per the Rabi period can be observed in conditional ionization spectra, independently on the presence [46] or absence [47] of an auto-ionizing level. Moreover, for the previously discussed systems, the dipole-dipole interaction leads to the generation of entangled states encompassing both the ionized and the bound electrons [48, 49]. The observed spectral correlations have been conveniently quantified by the density of quadratic negativity [50] defined in terms of partially transposed statistical operators [51, 52]. Moreover, it has been shown that the dipole-dipole interaction does not suppress the occurrence of the Fano zero in general, but its existence is restricted to only rather special conditions [53, 54]. Also a quantized field has been considered for the two-atom auto-ionizing model showing that many sharp peaks in the ionization spectra originating in discrete field energies can occur [49].

It will be shown that the exact Fano zeroes typical for ionization spectra of individual atoms cannot occur in the analyzed model of two auto-ionization systems. On the other hand, many spectral features found in the Fano model of an auto-ionization system [14] are present in the analyzed system including sharp peaks and dips. The applied algebraic approach provides analytical formulas that allow to get a deep insight into the behavior of two interacting auto-ionization subsystems analyzing spectral correlations and entanglement [55] of the state of two ionized electrons. Similarly as in [48] the density of quadratic negativity is applied to quantify quantum spectral correlations. Although the model is discussed in general using the values of parameters emphasizing its main features, the values of parameters suitable for molecular condensates (including molecular crystals)

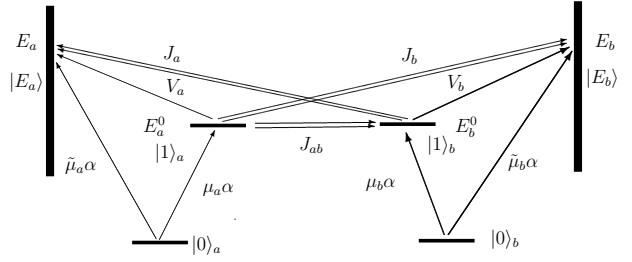


**Figure 1.** Scheme of the mutually interacting auto-ionization systems  $a$  and  $b$ . State  $|1\rangle_j$  denotes an excited bound state of atom  $j$  with energy  $E_j$  whereas state  $|E_j\rangle$  with energy  $E_j$  lies inside the continuum of atom  $j$ ,  $j = a, b$ . Symbols  $\mu_j$  and  $\tilde{\mu}_j$  stand for the dipole moments between the ground state  $|0\rangle_j$  and the corresponding excited states,  $\alpha_L$  stands for the pumping amplitude,  $V_j$  describes the Coulomb configuration coupling between states  $|1\rangle_j$  and  $|E_j\rangle$ . Symbols  $J_{ab}$ ,  $J_a$  and  $J_b$  refer to the dipole-dipole interactions between the excited/ionized states at atoms  $a$  and  $b$  indicated in the scheme. Double arrows mean that two electrons at atoms  $a$  and  $b$  participate in the interaction leading to energy transfer.

[56] are also considered.

The paper is organized as follows. Hamiltonian of two coupled auto-ionization systems in a stationary optical field is given in Sec. 2, together with the corresponding dynamical equations and their solution. Quadratic negativity and its density as quantifiers of entanglement between two ionized electrons is introduced in Sec. 3. Long-time photoelectron ionization spectra for the cases of comparable direct and indirect ionization paths (Subsec. 4.1) and dominating indirect ionization path (Subsec. 4.2) are analyzed in Sec. 4. Entanglement in the long-time photoelectron spectra is discussed in Sec. 5. Sec. 6 is devoted to the process of ionization in molecular condensates. Sec. 7 brings conclusions. Analytical solution of the model without the mutual interaction is provided in Appendix A. Appendix B is devoted to the competition of the dipole-dipole interactions between discrete auto-ionizing levels and with the continua.

## 2. Hamiltonian, dynamical equations and their solution

We consider two auto-ionization systems describing, e.g., two atoms or molecules that mutually interact by the dipole-dipole interaction (for the scheme, see Fig. 1). Both the ionization systems denoted as  $a$  and  $b$  are assumed to have one auto-ionizing level. They interact with a stationary optical field with amplitude  $\alpha_L$  and frequency  $E_L$  through the corresponding dipole moments. Hamiltonian  $\hat{H}_j$  describing auto-ionization system  $j$ ,  $j = a, b$ , can be written as ( $\hbar = 1$  is assumed, [57]):

$$\hat{H}_j = \hat{H}_j^0 + \hat{H}_j^L, \quad j = a, b, \quad (1)$$

$$\hat{H}_j^0 = E_j^0 |1\rangle_j \langle 1| + \int dE_j E_j |E_j\rangle \langle E_j| + \int dE_j [V_j |E_j\rangle \langle 1| + \text{H.c.}], \quad (2)$$

$$\hat{H}_j^L = [\mu_j \alpha_L \exp(-iE_L t) |1\rangle_j \langle 0| + \int dE_j \tilde{\mu}_j \alpha_L \exp(-iE_L t) |E_j\rangle \langle 0| + \text{H.c.}]. \quad (3)$$

In Eqs. (1–3), Hamiltonian  $\hat{H}_j^0$  describes the inner structure of auto-ionization system  $j$  whereas Hamiltonian  $\hat{H}_j^L$  arises from the interaction of the system with the optical field. Symbol  $E_j^0$  denotes the excitation energy from the ground state  $|0\rangle_j$  into the excited bound state  $|1\rangle_j$  of atom  $j$ . The continuum of atom  $j$  is formed by states  $|E_j\rangle$  having energies  $E_j$ . The Coulomb configuration interaction between states  $|1\rangle_j$  and  $|E_j\rangle$  inside the continuum is described by coupling constant  $V_j$ . Dipole moments  $\mu_j$  and  $\tilde{\mu}_j$  characterize an optical excitation of the corresponding states. Symbol H.c. stands for the Hermitian conjugated term.

The dipole-dipole interaction between atoms  $a$  and  $b$  leads to energy transfer [56]. It can be described by the following Hamiltonian  $\hat{H}_{\text{trans}}$ :

$$\hat{H}_{\text{trans}} = [J_{ab} |0\rangle_a |1\rangle_b \langle 0|_a \langle 1| + \int dE_a J_a |E_a\rangle |0\rangle_b \langle 1|_a \langle 0| + \int dE_b J_b |0\rangle_a |E_b\rangle_b \langle 0|_a \langle 1| + \text{H.c.}]. \quad (4)$$

In this interaction, one electron loses its energy and returns into its ground state, whereas the other electron takes this energy and moves into its own excited/ionized state. Constant  $J_{ab}$  describes the interaction between excited states  $|1\rangle_a$  and  $|1\rangle_b$  whereas constant  $J_a$  [ $J_b$ ] characterizes the interaction between excited state  $|1\rangle_b$  [ $|1\rangle_a$ ] and ionized states  $|E_a\rangle$  [ $|E_b\rangle$ ]. We assume that the electrons in ionized states do not mutually interact.

A general quantum state of two electrons at atoms  $a$  and  $b$  written in the frame rotating with frequency  $E_L$  can be expressed as:

$$|\psi\rangle(t) = c_{00}(t) |0\rangle_a |0\rangle_b + c_{10}(t) |1\rangle_a |0\rangle_b + c_{01}(t) |0\rangle_a |1\rangle_b + c_{11}(t) |1\rangle_a |1\rangle_b + \int dE_a [d_{a,0}(E_a, t) |E_a\rangle |0\rangle_b + d_{a,1}(E_a, t) |E_a\rangle |1\rangle_b] + \int dE_b [d_{b,0}(E_b, t) |0\rangle_a |E_b\rangle + d_{b,1}(E_b, t) |1\rangle_a |E_b\rangle] + \int dE_a \int dE_b d(E_a, E_b, t) |E_a\rangle |E_b\rangle. \quad (5)$$

Time-dependent coefficients  $c_{00}$ ,  $c_{10}$ ,  $c_{01}$ ,  $c_{11}$ ,  $d_{a,0}(E_a)$ ,  $d_{a,1}(E_a)$ ,  $d_{b,0}(E_b)$ ,  $d_{b,1}(E_b)$ , and  $d(E_a, E_b)$  characterize the state  $|\psi\rangle$  at an arbitrary time

$t$ . They can be conveniently grouped into the vectors  $\mathbf{c}^T(t) = [c_{00}(t), c_{10}(t), c_{01}(t), c_{11}(t)]$  and  $\mathbf{d}_j^T(E_j, t) = [d_{j,0}(E_j, t), d_{j,1}(E_j, t)]$  for  $j = a, b$ . Symbol  $T$  denotes transposition. Normalization of the state  $|\psi\rangle(t)$  in Eq. (5) provides the relation  $\mathbf{c}^\dagger(t)\mathbf{c}(t) + \sum_{j=a,b} \int dE_j \mathbf{d}_j^\dagger(E_j, t)\mathbf{d}_j(E_j, t) + \int dE_a \int dE_b |d(E_a, E_b, t)|^2 = 1$ .

The Schrödinger equation with the overall Hamiltonian  $\hat{H}_a + \hat{H}_b + \hat{H}_{\text{trans}}$  provides the following dynamical equations for the coefficients characterizing state  $|\psi\rangle(t)$  written in Eq. (5):

$$i \frac{d}{dt} \begin{bmatrix} \mathbf{c}(t) \\ \mathbf{d}_a(E_a, t) \\ \mathbf{d}_b(E_b, t) \\ d(E_a, E_b, t) \end{bmatrix} = \begin{bmatrix} \mathbf{A} & \int dE_a \mathbf{B}_a \\ \mathbf{B}_a^\dagger & (E_a - E_L)\mathbf{1} + \mathbf{K}_b \\ \mathbf{B}_b^\dagger & \mathbf{0} \\ \mathbf{0} & \mathbf{I}_b^\dagger \\ \int dE_b \mathbf{B}_b & \mathbf{0} \\ \mathbf{0} & \int dE_b \mathbf{I}_b \\ (E_b - E_L)\mathbf{1} + \mathbf{K}_a & \int dE_a \mathbf{I}_a \\ \mathbf{I}_a^\dagger & E_a + E_b - 2E_L \end{bmatrix} \begin{bmatrix} \mathbf{c}(t) \\ \mathbf{d}_a(E_a, t) \\ \mathbf{d}_b(E_b, t) \\ d(E_a, E_b, t) \end{bmatrix}. \quad (6)$$

In Eq. (6), symbol  $\mathbf{1}$  ( $\mathbf{0}$ ) stands for the unity (zero) matrix of appropriate dimension(s).

Matrices  $\mathbf{A}$ ,  $\mathbf{B}_a$ ,  $\mathbf{B}_b$ ,  $\mathbf{K}_a$ ,  $\mathbf{K}_b$ ,  $\mathbf{I}_a$  and  $\mathbf{I}_b$  introduced in Eq. (6) are defined as follows:

$$\mathbf{A} = \begin{bmatrix} 0 & \mu_a^* \alpha_L^* & \mu_b^* \alpha_L^* & 0 \\ \mu_a \alpha_L & \Delta E_a^0 & J_{ab}^* & \mu_b^* \alpha_L^* \\ \mu_b \alpha_L & J_{ab} & \Delta E_b^0 & \mu_a^* \alpha_L^* \\ 0 & \mu_b \alpha_L & \mu_a \alpha_L & \Delta E_a^0 + \Delta E_b^0 \end{bmatrix}, \quad \mathbf{B}_a = \begin{bmatrix} \tilde{\mu}_a^* \alpha_L^* & 0 \\ V_a^* & 0 \\ J_a^* & \tilde{\mu}_a^* \alpha_L^* \\ 0 & V_a^* \end{bmatrix}, \quad \mathbf{B}_b = \begin{bmatrix} \tilde{\mu}_b^* \alpha_L^* & 0 \\ J_b^* & \tilde{\mu}_b^* \alpha_L^* \\ V_b^* & 0 \\ 0 & V_b^* \end{bmatrix}, \quad \mathbf{K}_j = \begin{bmatrix} 0 & \mu_j^* \alpha_L^* \\ \mu_j \alpha_L & \Delta E_j^0 \end{bmatrix}, \quad \mathbf{I}_j = \begin{bmatrix} \tilde{\mu}_j^* \alpha_L^* \\ V_j^* \end{bmatrix}, \quad j = a, b; \quad (7)$$

$$\Delta E_j^0 = E_j^0 - E_L, \quad j = a, b.$$

The set of equations (6) can be conveniently solved by the Laplace transform defined for an arbitrary function  $f(t)$  as  $\tilde{f}(\varepsilon) = \int_0^\infty dt f(t) \exp(i\varepsilon t)$ . If we assume that only the discrete levels of atoms  $a$  and  $b$  are initially populated, we arrive at the following set of equations:

$$[\varepsilon \mathbf{1} - \mathbf{A}] \tilde{\mathbf{c}}(\varepsilon) - \sum_{j=a,b} \int dE_j \mathbf{B}_j \tilde{\mathbf{d}}_j(E_j, \varepsilon) = i\mathbf{c}(0), \quad (8)$$

$$[(\varepsilon - E_a + E_L)\mathbf{1} - \mathbf{K}_b] \tilde{\mathbf{d}}_a(E_a, \varepsilon) - \mathbf{B}_a^\dagger \tilde{\mathbf{c}}(\varepsilon) - \int dE_b \mathbf{I}_b \tilde{d}(E_a, E_b, \varepsilon) = \mathbf{0}, \quad (9)$$

$$[(\varepsilon - E_b + E_L)\mathbf{1} - \mathbf{K}_a] \tilde{\mathbf{d}}_b(E_b, \varepsilon) - \mathbf{B}_b^\dagger \tilde{\mathbf{c}}(\varepsilon) - \int dE_a \mathbf{I}_a \tilde{d}(E_a, E_b, \varepsilon) = \mathbf{0}, \quad (10)$$

$$\begin{aligned}
&(\varepsilon - E_a - E_b + 2E_L)\tilde{d}(E_a, E_b, \varepsilon) \\
&\quad - \mathbf{I}_b^\dagger \tilde{\mathbf{d}}_a(E_a, \varepsilon) - \mathbf{I}_a^\dagger \tilde{\mathbf{d}}_b(E_b, \varepsilon) = 0. \quad (11)
\end{aligned}$$

Vector  $\mathbf{c}(0)$  occurring in Eq. (8) describes the initial condition. If the electrons at both atoms are initially in their ground states,  $\mathbf{c}^T(0) = [1, 0, 0, 0]$ .

Equations (8–11) can be solved as follows. First, using Eq. (11) we express function  $\tilde{d}(E_a, E_b, \varepsilon)$  in the following form:

$$\tilde{d}(E_a, E_b, \varepsilon) = \frac{\mathbf{I}_b^\dagger \tilde{\mathbf{d}}_a(E_a, \varepsilon) + \mathbf{I}_a^\dagger \tilde{\mathbf{d}}_b(E_b, \varepsilon)}{\varepsilon - E_a - E_b + 2E_L}. \quad (12)$$

Substitution of the expression (12) into Eqs. (9) and (10) and subsequent integration in these equations results in the following equations:

$$\begin{aligned}
&[(\varepsilon - E_a + E_L)\mathbf{1} + \mathbf{L}_b] \tilde{\mathbf{d}}_a(E_a, \varepsilon) \\
&\quad - \int dE_b \frac{\mathbf{I}_b \mathbf{I}_a^\dagger \tilde{\mathbf{d}}_b(E_b, \varepsilon)}{\varepsilon - E_a - E_b + 2E_L} = \mathbf{B}_a^\dagger \tilde{\mathbf{c}}(\varepsilon), \quad (13)
\end{aligned}$$

$$\begin{aligned}
&[(\varepsilon - E_b + E_L)\mathbf{1} + \mathbf{L}_a] \tilde{\mathbf{d}}_b(E_b, \varepsilon) \\
&\quad - \int dE_a \frac{\mathbf{I}_a \mathbf{I}_b^\dagger \tilde{\mathbf{d}}_a(E_a, \varepsilon)}{\varepsilon - E_a - E_b + 2E_L} = \mathbf{B}_b^\dagger \tilde{\mathbf{c}}(\varepsilon). \quad (14)
\end{aligned}$$

The newly defined  $2 \times 2$  matrices  $\mathbf{L}_a$  and  $\mathbf{L}_b$  are given as

$$\mathbf{L}_j = -\mathbf{K}_j + i\pi \mathbf{I}_j \mathbf{I}_j^\dagger, \quad j = a, b. \quad (15)$$

In the next step, we neglect the terms in Eqs. (13) and (14) containing the integrations over  $E_a$  and  $E_b$ . As shown in Appendix A these terms equal zero for independent atoms  $a$  and  $b$ . Weakness of the dipole-dipole interaction compared to the Coulomb one then justifies this approximation that leaves us the following decoupled equations:

$$[(\varepsilon - E_a + E_L)\mathbf{1} + \mathbf{L}_b] \tilde{\mathbf{d}}_a(E_a, \varepsilon) = \mathbf{B}_a^\dagger \tilde{\mathbf{c}}(\varepsilon), \quad (16)$$

$$[(\varepsilon - E_b + E_L)\mathbf{1} + \mathbf{L}_a] \tilde{\mathbf{d}}_b(E_b, \varepsilon) = \mathbf{B}_b^\dagger \tilde{\mathbf{c}}(\varepsilon). \quad (17)$$

These equations can be solved using the decomposition of matrices  $\mathbf{L}_a$  and  $\mathbf{L}_b$  [47],

$$\mathbf{L}_j = \sum_{k=1,2} \lambda_k^j \mathbf{L}_k^j, \quad j = a, b, \quad (18)$$

in which  $\lambda_k^j$  are eigenvalues of the matrix  $\mathbf{L}_j$  and matrices  $\mathbf{L}_1^j$  and  $\mathbf{L}_2^j$  fulfil the relation  $\mathbf{L}_1^j + \mathbf{L}_2^j = \mathbf{1}$ . Formulas for eigenvalues  $\lambda_k^j$  are derived as follows:

$$\lambda_{1,2}^j = a_1^j \pm \sqrt{a_1^{j2} - a_2^j}, \quad j = a, b; \quad (19)$$

$$a_1^j = [i\pi (|\tilde{\mu}_j \alpha_L|^2 + |V_j|^2) - \Delta E_j^0] / 2,$$

$$\begin{aligned}
a_2^j &= -i\pi |\tilde{\mu}_j \alpha_L|^2 \Delta E_j^0 - |\mu_j \alpha_L|^2 \\
&\quad + i\pi (\tilde{\mu}_j^* \mu_j |\alpha_L|^2 V_j + \text{c.c.}),
\end{aligned}$$

where c.c. denotes the complex conjugated term. Using eigenvalues  $\lambda_k^j$ , the matrices  $\mathbf{L}_k^j$  are expressed as:

$$\mathbf{L}_1^j = \frac{1}{\lambda_1^j - \lambda_2^j} (\mathbf{L}_j - \lambda_2^j \mathbf{1}), \quad \mathbf{L}_2^j = \mathbf{1} - \mathbf{L}_1^j. \quad (20)$$

Substitution of the decomposition (18) into Eq. (16) allows to obtain the solution of Eq. (16) in the simple form:

$$\tilde{\mathbf{d}}_a(E_a, \varepsilon) = \sum_{k=1,2} \frac{\mathbf{L}_k^b \mathbf{B}_a^\dagger \tilde{\mathbf{c}}(\varepsilon)}{\varepsilon - E_a + E_L + \lambda_k^b}. \quad (21)$$

The solution of Eq. (17) is derived from that written in Eq. (21) by the formal substitution  $a \leftrightarrow b$ .

Substitution of the solutions  $\tilde{\mathbf{d}}_a(E_a, \varepsilon)$  and  $\tilde{\mathbf{d}}_b(E_b, \varepsilon)$  into Eq. (8) and subsequent integration over energies  $E_a$  and  $E_b$  provides the equation

$$[\varepsilon \mathbf{1} - \bar{\mathbf{A}}] \tilde{\mathbf{c}}(\varepsilon) = i\mathbf{c}(0). \quad (22)$$

In Eq. (22), matrix  $\bar{\mathbf{A}}$  is defined as

$$\bar{\mathbf{A}} = \mathbf{A} - i\pi \sum_{j=a,b} \mathbf{B}_j \mathbf{B}_j^\dagger. \quad (23)$$

The solution of Eq. (22) can be conveniently written in terms of eigenvalues  $\Lambda_k$  and eigenvectors  $\mathbf{p}_k$  and  $\mathbf{p}_k^{-1}$  of the matrix  $\bar{\mathbf{A}}$  decomposed as  $\bar{\mathbf{A}} = \mathbf{P} \mathbf{\Lambda} \mathbf{P}^{-1}$ ,

$$\tilde{\mathbf{c}}(\varepsilon) = i \sum_{k=1}^4 \mathbf{p}_k \frac{[\mathbf{p}_k^{-1} \mathbf{c}(0)]}{\varepsilon - \Lambda_k}. \quad (24)$$

Whereas eigenvectors  $\mathbf{p}_k$  form columns of the matrix  $\mathbf{P}$ , eigenvectors  $\mathbf{p}_k^{-1}$  occur as rows of the inverse matrix  $\mathbf{P}^{-1}$ .

Substituting Eq. (24) into Eq. (21), coefficients  $\tilde{\mathbf{d}}_a(E_a, \varepsilon)$  are obtained in the form:

$$\tilde{\mathbf{d}}_a(E_a, \varepsilon) = i \sum_{j=1}^2 \sum_{k=1}^4 \frac{[\mathbf{L}_j^b \mathbf{B}_a^\dagger \mathbf{p}_k]}{\varepsilon - E_a + E_L + \lambda_j^b} \frac{[\mathbf{p}_k^{-1} \mathbf{c}(0)]}{\varepsilon - \Lambda_k}. \quad (25)$$

It can be shown by direct calculation that the integration over  $E_a$  in Eq. (14) using the solution (25) gives zero. Similarly, the solution for  $\tilde{\mathbf{d}}_b(E_b, \varepsilon)$  obtained from the symmetry  $a \leftrightarrow b$  results in zero after the integration in Eq. (13). This confirms consistency of the approximation leading to Eqs. (16) and (17).

Finally, using Eq. (25) the expression (12) for coefficients  $\tilde{d}(E_a, E_b, \varepsilon)$  is expressed as:

$$\begin{aligned}
\tilde{d}(E_a, E_b, \varepsilon) &= \frac{i}{\varepsilon - E_a - E_b + 2E_L} \left\{ \sum_{j=1}^2 \sum_{k=1}^4 \right. \\
&\quad \left. \frac{[\mathbf{I}_b^\dagger \mathbf{L}_j^b \mathbf{B}_a^\dagger \mathbf{p}_k]}{\varepsilon - E_a + E_L + \lambda_j^b} \frac{[\mathbf{p}_k^{-1} \mathbf{c}(0)]}{\varepsilon - \Lambda_k} + \{a \leftrightarrow b\} \right\}. \quad (26)
\end{aligned}$$

Symbol  $\{a \leftrightarrow b\}$  in Eq. (26) replaces the term obtained by the exchange of the indicated indices.

The inverse Laplace transform of the above formulas then provides the coefficients in the time domain. Equation (24) attains the following form:

$$\mathbf{c}(t) = \sum_{k=1}^4 \mathbf{p}_k [\mathbf{p}_k^{-1} \mathbf{c}(0)] \exp(-i\Lambda_k t). \quad (27)$$

Decomposition of rational functions into partial fractions followed by the Laplace transform leaves formula (25) as follows:

$$\mathbf{d}_a(E_a, t) = \sum_{j=1}^2 \sum_{k=1}^4 \frac{[\mathbf{L}_j^b \mathbf{B}_a^\dagger \mathbf{p}_k] [\mathbf{p}_k^{-1} \mathbf{c}(0)]}{E_a - E_L - \lambda_j^b - \Lambda_k} \times [\exp[-i(E_a - E_L - \lambda_j^b)t] - \exp(-i\Lambda_k t)]. \quad (28)$$

Similarly, equation (26) takes the following form in the time domain:

$$d(E_a, E_b, t) = \sum_{j=1}^2 \sum_{k=1}^4 \left\{ \frac{[\mathbf{I}_b^\dagger \mathbf{L}_j^b \mathbf{B}_a^\dagger \mathbf{p}_k] [\mathbf{p}_k^{-1} \mathbf{c}(0)]}{E_a + E_b - 2E_L - \Lambda_k} \times \left[ \frac{\exp(-i\Lambda_k t) - \exp[-i(E_a - E_L - \lambda_j^b)t]}{E_a - E_L - \lambda_j^b - \Lambda_k} + \frac{\exp[-i(E_a + E_b - 2E_L)t]}{E_b - E_L + \lambda_j^b} - \frac{\exp[-i(E_a - E_L - \lambda_j^b)t]}{E_b - E_L + \lambda_j^b} \right] + \{a \leftrightarrow b\} \right\}. \quad (29)$$

As eigenvalues  $\lambda_j^a$  and  $\lambda_j^b$  ( $\Lambda_k$ ) have positive (negative) imaginary parts, the above formulas considerably simplify in the long-time limit  $t \rightarrow \infty$ ,

$$\mathbf{c}^\infty(t) = [0, 0, 0, 0]^T,$$

$$\mathbf{d}_j^\infty(E_j, t) = [0, 0]^T, \quad j = a, b,$$

$$d^\infty(E_a, E_b, t) = \sum_{j=1}^2 \sum_{k=1}^4 \frac{[\mathbf{p}_k^{-1} \mathbf{c}(0)]}{E_a + E_b - 2E_L - \Lambda_k} \times \left\{ \frac{[\mathbf{I}_b^\dagger \mathbf{L}_j^b \mathbf{B}_a^\dagger \mathbf{p}_k]}{E_b - E_L + \lambda_j^b} + \frac{[\mathbf{I}_a^\dagger \mathbf{L}_j^a \mathbf{B}_b^\dagger \mathbf{p}_k]}{E_a - E_L + \lambda_j^a} \right\} \times \exp[-i(E_a + E_b - 2E_L)t]. \quad (30)$$

Both atoms are thus completely ionized in the long-time limit. In this limit, also the norm of the long-time joint photoelectron ionization spectrum  $|d^\infty(E_a, E_b)|^2$  is determined analytically,

$$\int dE_a \int dE_b |d^\infty(E_a, E_b)|^2 = 4\pi^2 \sum_{j, j'=1}^2 \sum_{k, k'=1}^4 \left\{ \frac{[\mathbf{I}_b^\dagger \mathbf{L}_j^b \mathbf{B}_a^\dagger \mathbf{p}_k]^* [\mathbf{I}_b^\dagger \mathbf{L}_{j'}^b \mathbf{B}_a^\dagger \mathbf{p}_{k'}]}{\lambda_j^{b*} - \lambda_{j'}^b} + \{a \leftrightarrow b\} \right\} \times \frac{[\mathbf{p}_k^{-1} \mathbf{c}(0)]^* [\mathbf{p}_{k'}^{-1} \mathbf{c}(0)]}{\Lambda_k^* - \Lambda_{k'}}. \quad (31)$$

As both atoms interact through the dipole-dipole interaction, energies  $E_a$  and  $E_b$  of the ionized electrons are correlated to some extent. This correlation is quantified by covariance  $C$  defined as:

$$C = \frac{\langle E_a E_b \rangle}{\sqrt{\langle E_a^2 \rangle \langle E_b^2 \rangle}}. \quad (32)$$

In Eq. (32), the mean values  $\langle E_a^k E_b^l \rangle$  for  $k, l \in N$  are defined as:

$$\langle E_a^k E_b^l \rangle = \int dE_a \int dE_b E_a^k E_b^l |d^\infty(E_a, E_b)|^2 \quad (33)$$

using the long-time joint photoelectron ionization spectrum  $|d^\infty(E_a, E_b)|^2$  determined in Eq. (30). As these correlations have quantum origin, they can alternatively be described by quadratic negativity as it is done in the following section.

### 3. Quadratic negativity for the composite system

We first consider a simplified model analyzed in [47, 46]. In this model, atom  $a$  has only two discrete states  $|0\rangle_a$  and  $|1\rangle_a$  whereas atom  $b$  contains the whole continuum  $|E_b\rangle$  of states with energies  $E_b$ . A general state  $|\psi_q\rangle$  of this system described by coefficients  $d_0(E_b)$  and  $d_1(E_b)$  takes the following form:

$$|\psi_q\rangle = \int dE_b [d_0(E_b)|0\rangle_a + d_1(E_b)|1\rangle_a] |E_b\rangle. \quad (34)$$

Quadratic negativity  $N_q$  quantifies the amount of non-separability of a state [50] as visible in negativity of the corresponding partially transposed statistical operator [51, 52]. It is determined by negative eigenvalues of the partially transposed statistical operator. Quadratic negativity of the state  $|\psi_q\rangle$  written in Eq. (34) has been derived in [48] in the form:

$$N_q = 2 \sum_{j, k=0}^1 \int dE_b \int dE'_b [d_j^*(E_b) d_j(E_b) d_k^*(E'_b) d_k(E'_b) - d_j^*(E_b) d_k(E_b) d_k^*(E'_b) d_j(E'_b)]. \quad (35)$$

Formula (35) can be recast as follows:

$$N_q = 2 \int dE_b \varrho_b(E_b) \int dE'_b \varrho_b(E'_b) n^q(E_b, E'_b), \quad (36)$$

where  $\varrho_b$  gives the density of states  $|E_b\rangle$  in the continuum of atom  $b$ :

$$\varrho_b(E_b) = \sum_{j=0}^1 |d_j(E_b)|^2. \quad (37)$$

Joint density of quadratic negativity  $n_q$  introduced in Eq. (36) is obtained in the form:

$$n_q(E_b, E'_b) = 1 - \frac{\sum_{j, k=0}^1 d_j^*(E_b) d_k(E_b) d_k^*(E'_b) d_j(E'_b)}{\varrho_b(E_b) \varrho_b(E'_b)}. \quad (38)$$

The joint density of quadratic negativity  $n_q$  gives quadratic negativity of the bipartite system formed by the states  $\{|0\rangle_a, |1\rangle_a\}$  and  $\{|E_b\rangle, |E'_b\rangle\}$ . According to Eq. (36), quadratic negativity  $N_q$  is given as a weighted sum of quadratic negativities between the two-level atom  $a$  and all possible pairs of states inside the continuum of atom  $b$ .

This interpretation suggests a straightforward generalization to the case of two continua substituting  $|0\rangle_a \rightarrow |E_a\rangle$  and  $|1\rangle_a \rightarrow |E'_a\rangle$  and integrating over frequencies  $E_a$  and  $E'_a$ :

$$N = \int dE_a \int dE'_a \int dE_b \int dE'_b [d^*(E_a, E_b)d(E_a, E_b)d^*(E'_a, E'_b)d(E'_a, E'_b) - d^*(E_a, E_b)d(E'_a, E_b)d^*(E'_a, E'_b)d(E_a, E'_b)]. \quad (39)$$

Coefficients  $d(E_a, E_b)$  determine a state  $|\psi\rangle$  common to both continua at atoms  $a$  and  $b$ :

$$|\psi\rangle = \int dE_a \int dE_b d(E_a, E_b)|E_a\rangle|E_b\rangle. \quad (40)$$

They also give densities  $\varrho_a$  and  $\varrho$  describing an ionized electron at atom  $a$  and both ionized electrons, respectively:

$$\begin{aligned} \varrho(E_a, E_b) &= |d(E_a, E_b)|^2, \\ \varrho_a(E_a) &= \int dE_b \varrho(E_a, E_b). \end{aligned} \quad (41)$$

Following the same argumentation as that applied earlier for the simplified model considered in [48], the joint density of quadratic negativity  $n$  can be introduced:

$$\begin{aligned} n(E_a, E'_a, E_b, E'_b) &= 2[\varrho_{ab}(E_a, E_b)\varrho_{ab}(E'_a, E'_b) \\ &\quad - d^*(E_a, E_b)d(E'_a, E_b)d^*(E'_a, E'_b)d(E_a, E'_b)] \\ &\quad \times \{\varrho_a(E_a)\varrho_a(E'_a)[\varrho_{ab}(E_a, E_b) + \varrho_{ab}(E'_a, E'_b)] \\ &\quad \times [\varrho_{ab}(E_a, E'_b) + \varrho_{ab}(E'_a, E'_b)]\}^{-1}. \end{aligned} \quad (42)$$

Quadratic negativity  $N$  can then be expressed using the densities  $\varrho_a$  and  $\varrho$  introduced in Eq. (41):

$$\begin{aligned} N &= \int dE_a \varrho_a(E_a) \int dE'_a \varrho_a(E'_a) \\ &\quad \times \int dE_b [\varrho(E_a, E_b) + \varrho(E'_a, E_b)] \\ &\quad \times \int dE'_b [\varrho(E_a, E'_b) + \varrho(E'_a, E'_b)] \\ &\quad \times n(E_a, E'_a, E_b, E'_b). \end{aligned} \quad (43)$$

Formula (43) can be recast into a simple form using the reduced statistical operator  $\tilde{\rho}_b$  of the continuum of atom  $b$ :

$$N = 2 \left[ 1 - \int dE_b \int dE'_b |\tilde{\rho}_b(E_b, E'_b)|^2 \right], \quad (44)$$

$$\tilde{\rho}_b(E_b, E'_b) = \int dE_a d(E_a, E_b)d^*(E_a, E'_b). \quad (45)$$

An analogous formula based on the reduced statistical operator of atom  $a$  can also be derived.

Another expression for quadratic negativity  $N$  can be reached using the Schmidt decomposition of state  $|\psi\rangle$  given in Eq. (40):

$$d(E_a, E_b) = \sum_n f_n(E_a)\lambda_n g_n(E_b); \quad (46)$$

$\lambda_n$  being coefficients of the decomposition. Functions  $f_n$  and  $g_n$  introduced in Eq. (46) form the dual orthonormal bases. Quadratic negativity  $N$  can then be determined according to the formula:

$$N = 2 \left[ 1 - \sum_n \lambda_n^4 \right]. \quad (47)$$

Any separable state gives  $N = 0$ , whereas we have  $N = 2(N_d - 1)/N_d$  for the maximally entangled state in  $N_d \times N_d$  dimensions. We note that the formula in Eq. (47) can be rewritten as  $N = 2(1 - 1/K)$  where  $K$  denotes the Schmidt number of independent modes.

We note that if atoms  $a$  and  $b$  contain also discrete levels the consideration of amplitude spectra with  $\delta$ -functions allows for easy incorporation of such levels into the above developed description (for details, see [48]).

Entanglement of two ionized electrons can easily be modified by filtering the energies of electrons. Quadratic negativity  $N_a$  characterizing a state with energies  $E_a$  of electron  $a$  in interval  $\langle E_a^0 - \Delta E, E_a^0 + \Delta E \rangle$  is obtained along the formula:

$$\begin{aligned} N_a(E_a^0) &= \mathcal{N}_a^{-2} \int_{E_a^0 - \Delta E}^{E_a^0 + \Delta E} dE_a \varrho_a(E_a) \int_{E_a^0 - \Delta E}^{E_a^0 + \Delta E} dE'_a \\ &\quad \varrho_a(E'_a) \int dE_b [\varrho_{ab}(E_a, E_b) + \varrho_{ab}(E'_a, E_b)] \\ &\quad \times \int dE'_b [\varrho_{ab}(E_a, E'_b) + \varrho_{ab}(E'_a, E'_b)] \\ &\quad \times n(E_a, E'_a, E_b, E'_b), \end{aligned} \quad (48)$$

$$\mathcal{N}_a = \int_{E_a^0 - \Delta E}^{E_a^0 + \Delta E} dE_a \int dE_b |d(E_a, E_b)|^2.$$

If also energies  $E_b$  of electron  $b$  are limited to interval  $\langle E_b^0 - \Delta E, E_b^0 + \Delta E \rangle$ , quadratic negativity  $N_{ab}$  of the resultant state is determined as follows:

$$\begin{aligned} N_{ab}(E_a^0, E_b^0) &= \mathcal{N}^{-2} \int_{E_a^0 - \Delta E}^{E_a^0 + \Delta E} dE_a \varrho_a(E_a) \int_{E_a^0 - \Delta E}^{E_a^0 + \Delta E} dE'_a \\ &\quad \varrho_a(E'_a) \int_{E_b^0 - \Delta E}^{E_b^0 + \Delta E} dE_b [\varrho_{ab}(E_a, E_b) + \varrho_{ab}(E'_a, E_b)] \\ &\quad \times \int_{E_b^0 - \Delta E}^{E_b^0 + \Delta E} dE'_b [\varrho_{ab}(E_a, E'_b) + \varrho_{ab}(E'_a, E'_b)] \\ &\quad \times n(E_a, E'_a, E_b, E'_b), \end{aligned} \quad (49)$$

$$\mathcal{N} = \int_{E_a^0 - \Delta E}^{E_a^0 + \Delta E} dE_a \int_{E_b^0 - \Delta E}^{E_b^0 + \Delta E} dE_b |d(E_a, E_b)|^2.$$

#### 4. Long-time photoelectron ionization spectra

In the following, we restrict ourselves to the most common case of two identical atoms. The discussion of photoelectron ionization spectra is divided into two parts according to the relative strength of direct

and indirect ionization paths. For the discussion, we introduce a useful parametrization that generalizes the parametrization introduced by Fano [14, 54]. In our parametrization, parameters  $\mu_j$ ,  $\tilde{\mu}_j$ ,  $V_j$ , and  $J_j$  ( $j = a, b$ ) are replaced by the following parameters [46]:

$$\begin{aligned} \gamma_j &= \pi|V_j|^2, & \bar{\gamma}_j &= \pi|J_j|^2, \\ q_j &= \frac{\mu_j}{\pi\tilde{\mu}_jV_j^*}, & \bar{q}_a &= \frac{\mu_b}{\pi\tilde{\mu}_aJ_a^*}, & \bar{q}_b &= \frac{\mu_a}{\pi\tilde{\mu}_bJ_b^*}, \\ \Gamma_j &= \gamma_j + \bar{\gamma}_j, & Q_j &= \frac{\gamma_jq_j + \bar{\gamma}_j\bar{q}_j}{\Gamma_j}, \end{aligned}$$

$$\Omega_j = \sqrt{4\pi\Gamma_j}(Q_j + i)\tilde{\mu}_j\alpha_L, \quad j = a, b. \quad (50)$$

In Eq. (50),  $\gamma_j$  ( $\bar{\gamma}_j$ ) gives damping of the continuum at atom  $j$  caused by the Coulomb (dipole-dipole) interaction and  $\Gamma_j$  is the overall damping. Parameter  $q_j$  ( $\bar{q}_j$ ) gives the ratio of indirect and direct ionization strengths related to the Coulomb (dipole-dipole) interaction. Parameter  $\Omega_j$  is linearly proportional to the pumping strength of ionization at atom  $j$ . As both atoms interact with the same laser field of amplitude  $\alpha_L$ , the introduction of two additional parameters is convenient:

$$m = \frac{\mu_b}{\mu_a}, \quad \Omega = \frac{\Omega_a + \Omega_b}{2}. \quad (51)$$

Whereas parameter  $m$  gives the ratio of dipole moments for the auto-ionizing states at both atoms, parameter  $\Omega$  describes average pumping strength. A suitable parametrization is based upon common parameters  $m$  and  $\Omega$  and parameters  $\gamma_j$ ,  $\bar{\gamma}_j$  and  $q_j$  of individual atoms defined in Eq. (50). We note that  $m = 1$  for two identical atoms and parameters  $\gamma_j$ ,  $q_j$  and  $\Omega_j = \Omega$ ,  $j = a, b$ , coincide with the usual ones defined by Fano [14].

#### 4.1. Spectra for comparable direct and indirect ionization paths

If the values of the Fano parameters  $q_a$  and  $q_b$  are close to the unity they characterize the case in which both ionization paths compete each other. This results in the creation of the Fano zeroes at energies  $E_a^0 - \gamma_a q_a$  and  $E_b^0 - \gamma_b q_b$  of electrons at atoms  $a$  and  $b$ , respectively. Individual spectra are formed by peaks that move down to lower energies with the increasing values of pumping parameter  $\Omega$ . Whereas the peaks are above the Fano energy for lower values of pumping parameter  $\Omega$ , they occur below the Fano energy for greater values of parameter  $\Omega$  [14]. As shown in Fig. 2(a) for ionization spectrum  $I_a$  of atom  $a$ , the dipole-dipole interaction with continuum (described by parameters  $J_a$  and  $J_b$ ) moves the peaks towards energies  $E_a^0$  and  $E_b^0$  of the auto-ionizing levels. This behavior reflects the fact that the dipole-dipole interaction with continuum itself ionizes atoms  $a$  and  $b$  and thus diminishes the contributions of direct

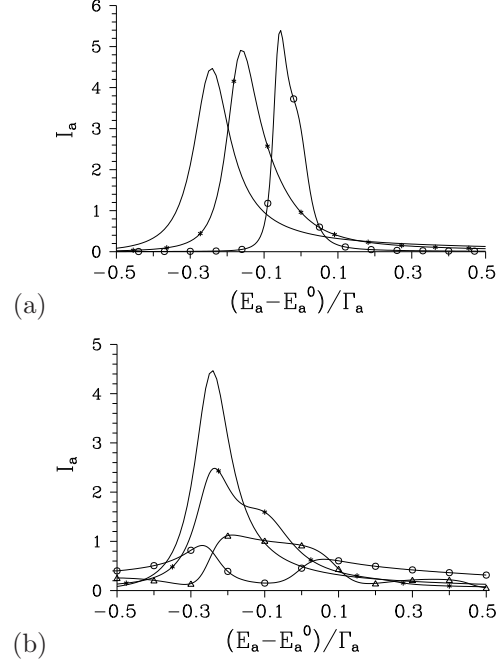


**Figure 2.** Long-time intensity photoelectron ionization spectrum  $I_a$  of atom  $a$  [ $I_a(E_a) = \int dE_b |d^\infty(E_a, E_b)|^2$ ] as a function of normalized energy  $(E_a - E_a^0)/\Gamma_a$  for (a)  $\bar{\gamma}_a = \bar{\gamma}_b = 0$  (independent atoms, curve without symbols), 0.1 (curve with \*), 1 (curve with  $\circ$ ),  $J_{ab} = 0$  and (b)  $J_{ab} = 0$  (independent atoms, curve without symbols), 0.56 (curve with \*), 1 (curve with  $\circ$ ), 1.68 (curve with  $\Delta$ ),  $\bar{\gamma}_a = \bar{\gamma}_b = 0$ ;  $E_a = E_b = E_L = 1$ ,  $q_a = q_b = 1$ ,  $\gamma_a = \gamma_b = 1$ ,  $\Omega = 1$ ,  $m = 1$ .

and indirect ionization paths whose interference is responsible for energy shifts of the peaks. On the other hand, the dipole-dipole interaction between the discrete auto-ionizing levels (described by parameter  $J_{ab}$ ) tends to form a peak close to energy  $E_a^0$  (or  $E_b^0$ ) in individual ionization spectra, as documented in Fig. 2(b). Two peaks coexist together in the spectra for intermediate values of parameter  $J_{ab}$ . If the dipole-dipole interaction between discrete auto-ionizing levels is sufficiently strong, there occurs one large peak in the photoelectron ionization spectrum  $I_a$  of atom  $a$  (or atom  $b$ ). It is separated by two minima from the tails built by the direct and indirect ionization paths. The presence of two minima in the spectrum reflects nontrivial mutual influence between the dipole-dipole interaction on one side and the direct and indirect ionization paths on the other side.

The dipole-dipole interaction mutually correlates energies of the ionized electrons at atoms  $a$  and  $b$  (see Fig. 3). This results in pure states of two ionized electrons entangled in energies  $E_a$  and  $E_b$ . Correlations increase with the increasing strength of both dipole-dipole interactions with the continua and between the discrete auto-ionizing levels. In fact, there occurs 'anti-correlation' between energies  $E_a$  and  $E_b$  of the

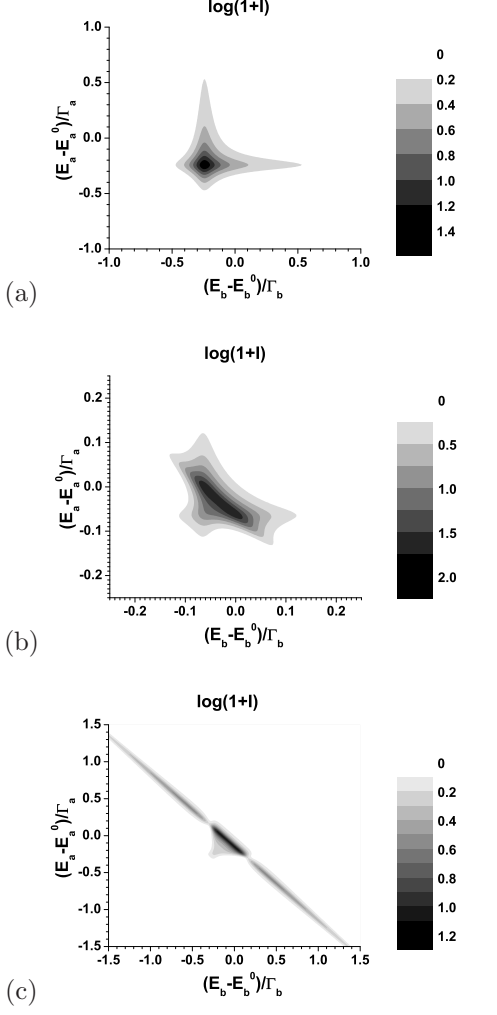


**Figure 3.** Topo graphs of long-time joint photoelectron ionization spectra  $I$  plotted as a function of normalized energies  $(E_a - E_a^0)/\Gamma_a$  and  $(E_b - E_b^0)/\Gamma_b$  of atoms  $a$  and  $b$ , respectively, for (a)  $\tilde{\gamma}_a = \tilde{\gamma}_b = 0$ ,  $J_{ab} = 0$  (independent atoms), (b)  $\tilde{\gamma}_a = \tilde{\gamma}_b = 1$ ,  $J_{ab} = 0$  and (c)  $\tilde{\gamma}_a = \tilde{\gamma}_b = 0$ ,  $J_{ab} = 1.68$ . Values of the other parameters are written in the caption to Fig. 2; log stands for decimal logarithm.

electrons that expresses the conservation law of energy in the stationary system ( $E_a + E_b \approx 2E_L$ ). Comparison of the joint photoelectron ionization spectra  $I$  plotted in Figs. 3(b) and (c) reveals that the stronger the dipole-dipole interaction the tighter the energy correlations.

If the dipole-dipole interactions with the continuum and between the discrete auto-ionizing levels have comparable strengths, a well-formed minimum occurs in the photoelectron ionization spectrum  $I_a$  ( $I_b$ ) of atom  $a$  ( $b$ ) (see Fig. 4). If the original spectra without the dipole-dipole interactions lie above the Fano zeros, intensity of this minimum is close to zero [see Fig. 4(a)]. If the original spectra are below the Fano zeros, the minimum intensity does not reach zero but

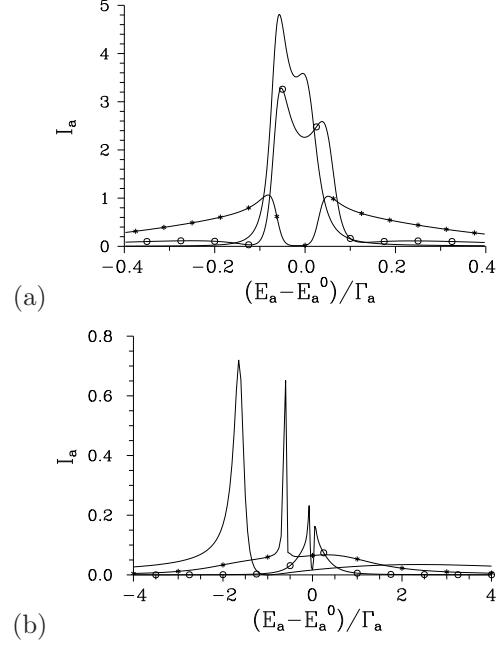


**Figure 4.** Long-time photoelectron ionization spectrum  $I_a$  of atom  $a$  for (a)  $J_{ab} = 0.56$  (curve without symbols), 2 (curve with \*), 4 (curve with  $\circ$ ),  $\tilde{\gamma}_a = \tilde{\gamma}_b = 1$ ,  $\Omega = 1$  and (b)  $\tilde{\gamma}_a = \tilde{\gamma}_b = 0$ ,  $J_{ab} = 0$  (independent atoms, curve without symbols),  $\tilde{\gamma}_a = \tilde{\gamma}_b = 1$ ,  $J_{ab} = 2$  (curve with  $\circ$ ),  $\Omega = 5$ . Values of the other parameters are written in the caption to Fig. 2. Curves with  $\tilde{\gamma}_a = \tilde{\gamma}_b = 1$  and  $J_{ab} = 2$  fulfil the 'balance condition' given in Eq. (B.10).

the intensity profile exhibits a sharp minimum accompanied by a neighbor sharp peak [see Fig. 4(b)]. Both cases give a clear evidence about the strong mutual influence of ionization channels based on the continuum and the discrete levels. Conditions for the balance of two ionization channels based on the dipole-dipole interaction have been found in Appendix B using the Fano diagonalization approach.

#### 4.2. Spectra for the dominating indirect ionization path

High values of the Fano parameters  $q_a$  and  $q_b$  occur in this region, in which the ionized states are reached nearly exclusively from discrete auto-ionizing levels with energies  $E_a^0$  and  $E_b^0$ . The individual photoelectron ionization spectra of both atoms thus consist of peaks centered around energy  $E_a^0$  ( $E_b^0$ ) for atom  $a$  ( $b$ ). There occurs the Autler-Townes splitting of these peaks [58] for intense pumping. It occurs whenever the speed of populating an auto-ionizing level is faster than its depletion due to the Coulomb configuration interaction ( $|\mu_a \alpha_L| > |V_a|$ ). As shown in Fig. 5 comparing the cases of independent and interacting atoms, the dipole-dipole interaction with the continuum weakens the Autler-Townes splitting.

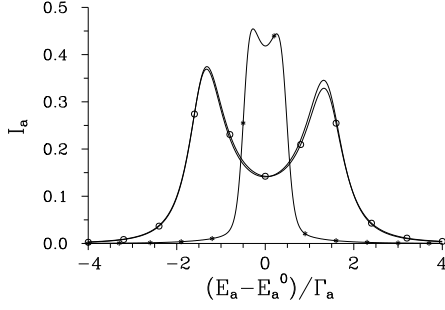


**Figure 5.** Long-time photoelectron ionization spectrum  $I_a$  of atom  $a$  for  $\tilde{\gamma}_a = \tilde{\gamma}_b = 0$ ,  $J_{ab} = 0$  (independent atoms, curve without symbols),  $\tilde{\gamma}_a = \tilde{\gamma}_b = 1$ ,  $J_{ab} = 0$  (curve with  $*$ ) and  $\tilde{\gamma}_a = \tilde{\gamma}_b = 0$ ,  $J_{ab} = 0.56$  (curve with  $\circ$ );  $E_a = E_b = E_L = 1$ ,  $q_a = q_b = 100$ ,  $\gamma_a = \gamma_b = 1$ ,  $\Omega = 3$ ,  $m = 1$ .

This is a consequence of the fact that the dipole-dipole interaction makes the transfer of electrons from discrete excited auto-ionizing levels into their continua faster and so partly suppresses the effect of 'population reversion' at the discrete auto-ionizing levels responsible for the splitting. On the other hand, the dipole-dipole interaction between the discrete auto-ionizing levels only slightly modifies the ionization spectra, as documented in Fig. 5. This follows from the considered symmetric configuration of atoms  $a$  and  $b$  that minimizes the influence of parameter  $J_{ab}$  to the populations of discrete levels  $E_a^0$  and  $E_b^0$ .

The dipole-dipole interaction with the continuum strongly modifies the joint photoelectron ionization spectra  $I$  that belong to the states entangled in energies. Dramatic change of the joint photoelectron ionization spectrum  $I$  caused by this interaction is illustrated in Fig. 6 in which the dipole-dipole interaction nearly completely suppresses the Autler-Townes splitting.

## 5. Entanglement in long-time photoelectron ionization spectra

The joint photoelectron ionization spectra  $I$  plotted in Figs. 3(b) and (c) and 6(b) reflect strong correlations in energies  $E_a$  and  $E_b$  of the ionized electrons created due to the dipole-dipole interaction. These correlations emerging during the quantum evolution are non-classical. They reflect the bipartite entanglement that can be quantified by quadratic negativity  $N$  introduced in Sec. 3. Alternatively, they can be described by the von Neumann entropy  $S$  of the reduced statistical operators of individual electrons  $a$  and  $b$ . We note that entropy  $S$  is a monotonous function of negativity  $N$ . Contrary to entropy, quadratic negativity  $N$  can be expressed via its joint density  $n$  introduced in Eq. (41). This represents an important advantage as it allows to connect entanglement with spectral properties of the

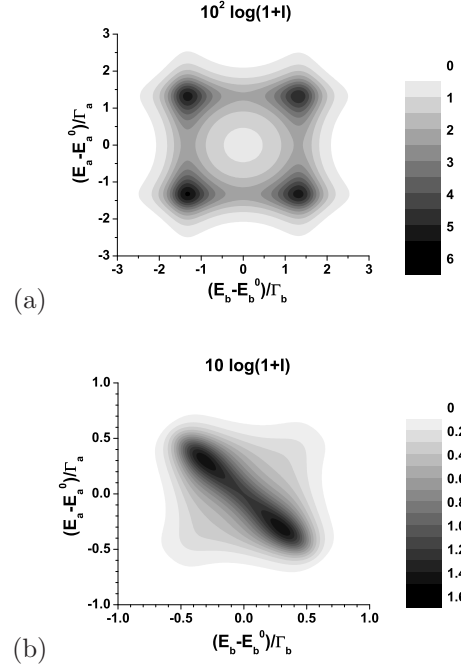


**Figure 6.** Topo graphs of long-time joint photoelectron ionization spectra  $I$  for (a)  $\tilde{\gamma}_a = \tilde{\gamma}_b = 0$  (independent atoms) and (b)  $\tilde{\gamma}_a = \tilde{\gamma}_b = 1$ ;  $J_{ab} = 0$  and values of the other parameters are written in the caption to Fig. 5.

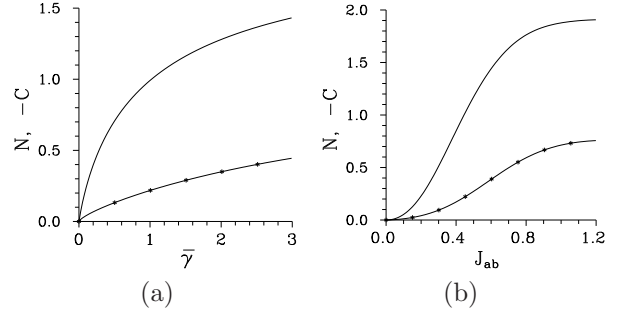


**Figure 7.** Quadratic negativity  $N$  (curve without symbols) and covariance  $C$  (curve with  $*$ ) as they depend on (a) parameter  $\tilde{\gamma} \equiv \tilde{\gamma}_a = \tilde{\gamma}_b$  and (b) parameter  $J_{ab}$ . Values of the other parameters are written in the caption to Fig. 2.

ionized electrons.

Assuming other parameters fixed, the increasing values of parameters  $J_a$  ( $\tilde{\gamma}_a$ ) and  $J_b$  ( $\tilde{\gamma}_b$ ) describing the dipole-dipole interactions with the continua result in greater values of negativity  $N$  [see Fig. 7(a)]. Similarly, the greater the values of parameter  $J_{ab}$  characterizing the dipole-dipole interaction between the discrete auto-ionizing levels, the greater the values of negativity  $N$  [see Fig. 7(b)]. In Fig. 7, the comparison of curves giving negativity  $N$  and covariance  $C$  of energies reveals that even the classical covariance  $C$  can be used as a good indicator of mutual coupling of two ionized electrons.

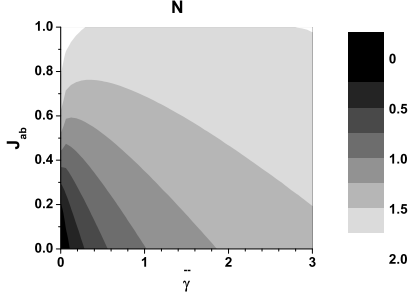


**Figure 8.** Topo graph of quadratic negativity  $N$  as it depends on dipole-dipole interaction parameters  $\tilde{\gamma} \equiv \tilde{\gamma}_a = \tilde{\gamma}_b$  and  $J_{ab}$ . Values of the parameters are written in the caption to Fig. 2.

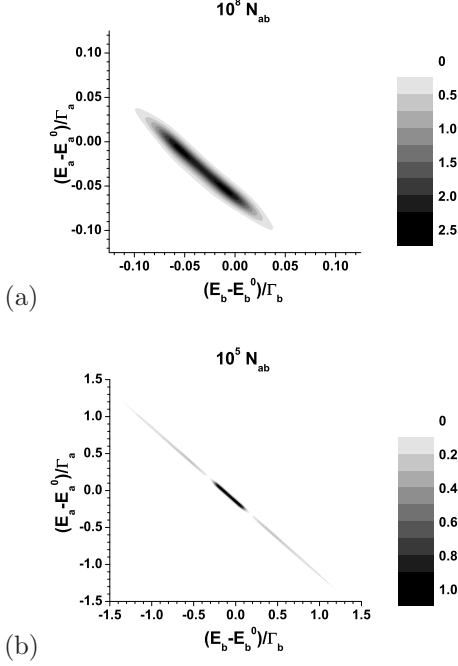


**Figure 9.** Topo graphs of quadratic negativity  $N_{ab}$  depending on normalized energies  $(E_a - E_a^0)/\Gamma_a$  and  $(E_b - E_b^0)/\Gamma_b$  for (a)  $\tilde{\gamma}_a = \tilde{\gamma}_b = 1$ ,  $J_{ab} = 0$ ,  $\Delta E = 0.005$  [ $N = 0.98$ ] and (b)  $\tilde{\gamma}_a = \tilde{\gamma}_b = 0$ ,  $J_{ab} = 1.68$ ,  $\Delta E = 0.01$  [ $N = 1.79$ ]. Values of the other parameters are written in the caption to Fig. 2.

Whereas the dipole-dipole interactions with the continua and between the discrete auto-ionizing levels influence the ionization spectra in general in a complex way, they support each other in creating entanglement, as documented in Fig. 8.

Spectral distribution of entanglement can be conveniently visualized using negativity  $N_{ab}$  defined in Eq. (49). It characterizes a common state of both ionized electrons obtained by filtering the energies of electrons. The comparison of graphs shown in Figs. 9(a) and 6(b) and also in Figs. 9(b) and 3(c) reveals that the negativity  $N$  is concentrated in the areas with higher intensities.

Also when the energy of only one electron is

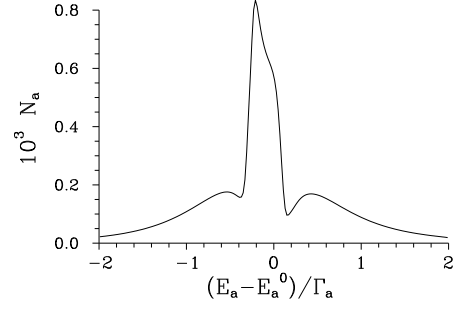


**Figure 10.** Quadratic negativity  $N_a$  as a function of normalized energy  $(E_a - E_a^0)/\Gamma_a$  of atom  $a$ ;  $\Delta E = 0.01$ ,  $J_{ab} = 1.68$  and values of the other parameters are written in the caption to Fig. 2;  $N = 1.79$ .

filtered, highly entangled states are obtained in the central part of the spectrum (see Fig. 10 for negativity  $N_a$ ). We note that the values of negativity  $N_{ab}$  as well as negativity  $N_a$  depend on the length  $\Delta E$  of the interval of measured energies [see Eqs. (48) and (49)]. The wider the interval  $\Delta E$  the greater the values of negativities. However, this dependence is weak.

## 6. Ionization in molecular condensates

The dipole-dipole interaction is usually much weaker than the dipole interaction of atoms or molecules with external coherent fields. It is also much weaker than the Coulomb configuration interaction. This means that only weak modifications of the ionization spectra discussed in Sec. 4 are expected in real systems. For example, energy shifts of the ionization peaks in the spectra plotted in Fig. 2 are comparable to the value of the dipole-dipole interaction energy. On the other hand, strongly correlated pairs of ionized electrons can be obtained in real systems provided that the process of ionization is sufficiently slow compared to the timescale characterizing the dipole-dipole interaction.

Molecular condensates [56] represent a typical example. In molecular crystals, energies of discrete excited states are in 1 eV, Coulomb configuration interaction energies in 10 meV and dipole-dipole interaction energies in  $0.1 \sim 1$  meV. Typical values of dipole moments are expressed in 1 D. Electric-field amplitudes in  $1 \times 10^8$  V/m are thus necessary to arrive at comparable dipole and Coulomb configuration interaction energies needed for the observation of the Autler-Townes splitting. If the Coulomb configuration interaction energy ( $V_a$ ) and the direct dipole interaction energy ( $\tilde{\mu}_a \alpha_L$ ) have equal strengths, also the ionization process considerably slows down. Electrons then tend to occupy their ground states and discrete auto-ionizing states, i.e. states mutually interacting through the dipole-dipole interaction. Alternatively, the electrons can undergo

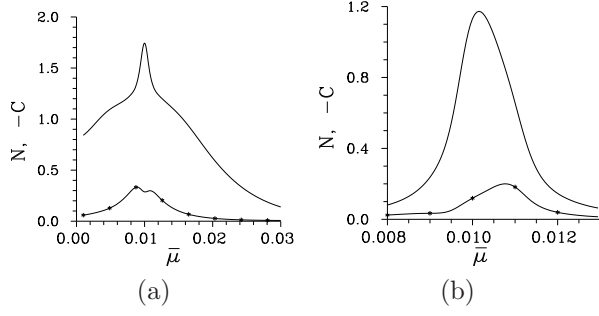


**Figure 11.** Quadratic negativity  $N$  (curve without symbols) and covariance  $C$  (curve with  $*$ ) as they depend on dipole moments  $\tilde{\mu} \equiv \tilde{\mu}_a = \tilde{\mu}_b$  for (a)  $J_a = J_b = 0.001$ ,  $J_{ab} = 0$  and (b)  $J_{ab} = 0.001$ ,  $J_a = J_b = 0$ ;  $E_a = E_b = E_L = 1$ ,  $\mu_a = \mu_b = 0.001$ ,  $V_a = V_b = 0.01$ ,  $\alpha_L = 1$ .

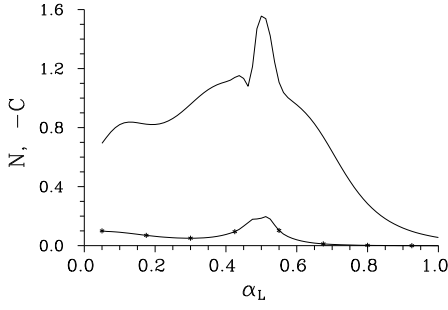


**Figure 12.** Quadratic negativity  $N$  (curve without symbols) and covariance  $C$  (curve with  $*$ ) depending on pump-field amplitude  $\alpha_L$ ;  $E_a = E_b = E_L = 1$ ,  $\mu_a = \mu_b = 0.001$ ,  $V_a = V_b = 0.01$ ,  $\tilde{\mu}_a = \tilde{\mu}_b = 0.02$ ,  $J_{ab} = 2 \times 10^{-4}$ ,  $J_a = J_b = 0$ .

ionization caused by the dipole-dipole interaction with the continua. In both cases, the influence of dipole-dipole interaction to the ionization process dramatically increases. This results in greater values of negativities  $N$  [see Fig. 11(a) for the interaction with the continua and Fig. 11(b) for the interaction between the auto-ionizing levels].

Considering fixed values of parameters  $V$  and  $\tilde{\mu}$ , the conditions maximizing negativity  $N$  and discussed above can be reached choosing suitably the pump-field amplitude  $\alpha_L$ . This is possible because negativity  $N$  as a function of pump-field amplitude  $\alpha_L$  exhibits a well-formed maximum (see Fig. 12).

## 7. Conclusions

Analytical solution of the model of two auto-ionization systems interacting through the dipole-dipole interaction has been found using the Laplace transform of the dynamical equations. Quadratic negativity together with its spectral density have been defined to quantify entanglement between two ionized electrons developed due to the dipole-dipole interaction. The dipole-dipole interaction with the

continua weakens the interference of direct and indirect ionization paths. This results in spectral shifts of the peaks in the long-time photoelectron ionization spectra towards the energy of the auto-ionizing state. On the other hand, the dipole-dipole interaction between the auto-ionizing states leads to the occurrence of an additional peak in the long-time photoelectron ionization spectra centered at the energy of the auto-ionizing state. When the auto-ionizing states play a dominant role in ionization and a strong pump field induces the Autler-Townes splitting of the ionization peak, the dipole-dipole interaction with the continua weakens this splitting. Balance of the dipole-dipole interactions with the continua and between the auto-ionizing states leads to the occurrence of a minimum in the long-time photoelectron ionization spectrum of an individual atom that resembles the Fano zero. The dipole-dipole interactions are responsible for strong anti-correlations in energies of the ionized electrons. They originate in the energy conservation. Both dipole-dipole interactions participate together in the creation of entanglement. The stronger the dipole-dipole interactions are the more entangled the state is. Optimal conditions for entanglement creation occur when the direct and indirect ionization paths are balanced and slow ionization is observed. 'Distribution of entanglement' in the state of two ionized electrons as described by the density of quadratic negativity reflects the shape of the corresponding joint photoelectron ionization spectrum.

## Acknowledgments

J.P. and A.L. gratefully acknowledge the support by the project LO1305 of the Ministry of Education, Youth and Sports of the Czech Republic. J.P. and W.L. also thank Operational Program Education for Competitiveness - European Social Fund project CZ.1.07/2.3.00/20.0058 of the Ministry of Education, Youth and Sports of the Czech Republic. A.L. thanks the project IGA No. PrF/2014/005. W.L. acknowledges Vietnam Ministry of Education Grant No. B2014-42-29 for support.

## Appendix A. Solution for two independent auto-ionization systems

If atoms  $a$  and  $b$  are independent the quantum state  $|\psi\rangle(t)$  in Eq. (5) can be written as

$$|\psi\rangle^{\text{ind}}(t) = |\psi_a\rangle(t)|\psi_b\rangle(t). \quad (\text{A.1})$$

In Eq. (A.1) states  $|\psi_j\rangle(t)$ ,  $j = a, b$ , describe electrons at individual atoms:

$$|\psi_j\rangle(t) = c_0^j(t)|0\rangle_j + c_1^j(t)|1\rangle_j + \int dE_j d_j(E_j, t)|E_j\rangle. \quad (\text{A.2})$$

The corresponding differential equations for the coefficients in Eq. (A.2) are derived as follows:

$$i \frac{d}{dt} \begin{bmatrix} \mathbf{c}_j(t) \\ d_j(E_j, t) \end{bmatrix} = \begin{bmatrix} \mathbf{K}_j & \int dE_j \mathbf{I}_j \\ \mathbf{I}_j^\dagger & E_j - E_L \end{bmatrix} \begin{bmatrix} \mathbf{c}_j(t) \\ d_j(E_j, t) \end{bmatrix} \quad (\text{A.3})$$

using vectors  $\mathbf{c}_j$ ,  $\mathbf{c}_j^T = (c_0^j, c_1^j)$  for  $j = a, b$ , and matrices  $\mathbf{K}_j$  and  $\mathbf{I}_j$  defined in Eq. (7).

The Laplace transform leaves equations (A.3) in the form:

$$\begin{aligned} [\varepsilon \mathbf{1} - \mathbf{K}_j] \tilde{\mathbf{c}}_j(\varepsilon) - \int dE_j \mathbf{I}_j \tilde{d}_j(E_j, \varepsilon) &= ic_j(0), \\ (\varepsilon - E_j + E_L) \tilde{d}_j(E_j, \varepsilon) - \mathbf{I}_j^\dagger \tilde{\mathbf{c}}_j(\varepsilon) &= 0, \quad j = a, b. \end{aligned} \quad (\text{A.4})$$

Applying the approach similar to that used in Sec. 2 the solution of Eqs. (A.4) is revealed in the form:

$$\begin{aligned} \tilde{\mathbf{c}}_j(\varepsilon) &= i \sum_{k=1,2} \frac{\mathbf{L}_k^j \mathbf{c}_j(0)}{\varepsilon + \lambda_k^j}, \\ \tilde{d}_j(E_j, \varepsilon) &= \frac{i}{\varepsilon - E_j + E_L} \sum_{k=1,2} \frac{\mathbf{I}_j^\dagger \mathbf{L}_k^j \mathbf{c}_j(0)}{\varepsilon + \lambda_k^j}, \quad j = a, b. \end{aligned} \quad (\text{A.5})$$

Matrices  $\mathbf{L}_k^j$  and eigenvalues  $\lambda_k^j$  used in Eq. (A.5) are given in Eqs. (19) and (20), respectively. The inverse Laplace transform provides this solution in the time domain:

$$\begin{aligned} \mathbf{c}_j(t) &= \sum_{k=1,2} \mathbf{L}_k^j \mathbf{c}_j(0) \exp(i\lambda_k^j t), \\ d_j(E_j, t) &= \sum_{k=1,2} \frac{\mathbf{I}_j^\dagger \mathbf{L}_k^j \mathbf{c}_j(0)}{E_j - E_L + \lambda_k^j} \left\{ \exp[-i(E_a - E_L)t] \right. \\ &\quad \left. - \exp(i\lambda_k^j t) \right\}, \quad j = a, b. \end{aligned} \quad (\text{A.6})$$

Considering the common state  $|\psi\rangle^{\text{ind}}$  of both atoms defined in Eq. (A1), the Laplace transform of coefficients  $\mathbf{c}(t)$  defined by direct product  $\mathbf{c}_a(t) \otimes \mathbf{c}_b(t)$  is expressed as:

$$\tilde{\mathbf{c}}(\varepsilon) = i \sum_{k,k'=1,2} \frac{[\mathbf{L}_k^a \mathbf{c}_a(0)] [\mathbf{L}_{k'}^b \mathbf{c}_b(0)]}{\varepsilon + \lambda_k^a + \lambda_{k'}^b}. \quad (\text{A.7})$$

Similarly, the Laplace transform of coefficients  $\mathbf{d}_a(E_a, t)$  determined by direct product  $\mathbf{c}_b(t) \otimes d_a(E_a, t)$  takes the form:

$$\begin{aligned} \tilde{\mathbf{d}}_a(E_a, \varepsilon) &= i \sum_{k,k'=1,2} \frac{[\mathbf{I}_a^\dagger \mathbf{L}_k^a \mathbf{c}_a(0)] [\mathbf{L}_{k'}^b \mathbf{c}_b(0)]}{E_a - E_L + \lambda_k^a} \\ &\quad \times \left[ \frac{1}{\varepsilon - E_a + E_L + \lambda_{k'}^b} - \frac{1}{\varepsilon + \lambda_k^a + \lambda_{k'}^b} \right]. \end{aligned} \quad (\text{A.8})$$

Using solutions (A.7) and (A.8), the first term in Eq. (13) can be treated as follows:

$$[(\varepsilon - E_a + E_L) \mathbf{1} + \mathbf{L}_b] \tilde{\mathbf{d}}_a(E_a, \varepsilon) =$$

$$\begin{aligned} &\sum_{k=1,2} (\varepsilon - E_a + E_L + \lambda_k^b) \mathbf{L}_k^b \tilde{\mathbf{d}}_a(E_a, \varepsilon) = \\ &i \sum_{k,k'=1,2} \frac{[\mathbf{I}_a^\dagger \mathbf{L}_k^a \mathbf{c}_a(0)] [\mathbf{L}_{k'}^b \mathbf{c}_b(0)]}{\varepsilon + \lambda_k^a + \lambda_{k'}^b} = \mathbf{B}_a^\dagger \tilde{\mathbf{c}}(\varepsilon). \end{aligned} \quad (\text{A.9})$$

The following relations have been used in Eq. (A.9),

$$\mathbf{L}_k^a \mathbf{L}_{k'}^a = \delta_{kk'} \mathbf{L}_k^a, \quad \mathbf{B}_a = \begin{bmatrix} \mathbf{I}_a & \mathbf{0} \\ \mathbf{0} & \mathbf{I}_a \end{bmatrix}. \quad (\text{A.10})$$

The equality expressed in Eq. (A.9) implies that the integral term in Eq. (13) is zero when independent atoms  $a$  and  $b$  are considered. The same holds also for the integral term in Eq. (14) owing to the symmetry  $a \leftrightarrow b$ . We note that this conclusion can be achieved also by direct integration of the solution written in Eq. (A.8).

## Appendix B. Competition of the discrete and continuum dipole-dipole interactions

Spectra in auto-ionization systems are formed by mutual interference of two types of ionization paths. One of them is based upon direct ionization originating from the ground state. The other uses an excited auto-ionizing discrete level that mediates auto-ionization of the system. These two ionization paths may interfere destructively. The presence of the Fano zero in the ionization spectra [14] represents a clear evidence of such quantum interference. Similarly, the dipole-dipole interaction of an auto-ionization system with its neighbor can be divided into two parts [46]. One part influences the discrete auto-ionizing level, states of the continuum are modified by the other. Also these two parts of the interaction compete. However, this competition occurs at the level of population of the involved quantum states as the dipole-dipole interaction means energy transfer. This competition naturally modifies photoelectron spectra. The greatest changes in photoelectron spectra are observed when both parts of the dipole-dipole interaction have comparable strengths. Suitable conditions for this case can be revealed as follows. First, we apply the usual Fano unitary transformations of excited/ionized states at atoms  $a$  and  $b$ . The appropriate values of parameters are then found from the requirement that the interaction Hamiltonian  $\hat{H}_{\text{trans}}$  given in Eq. (4) is zero. In this case, two parts of the dipole-dipole interaction related to the discrete and continuum states of both atoms are equally strong but with the opposed signs.

Invoking the Fano unitary transformations [14, 54] on both atoms, Hamiltonians  $\hat{H}_j^0$  written in Eq. (2) are transformed into their diagonal forms,

$$\hat{H}_j^0 = \int dE_j E_j |E_j\rangle \langle E_j|, \quad j = a, b. \quad (\text{B.1})$$

In Eq. (B.1), states  $|E_j\rangle$  arise from the Fano diagonalization,

$$|E_j\rangle = f_j(E_j)|1\rangle_j + \int dE'_j g_j(E_j, E'_j)|E'_j\rangle, \quad j = a, b \quad (\text{B.2})$$

and

$$f_j(E_j) = \frac{V_j^*(E_j)}{E_j - \tilde{E}_j^0 + i\gamma_j},$$

$$g_j(E_j, E'_j) = \frac{V_j(E'_j)f_j(E_j)}{E_j - E'_j + i\epsilon} + \delta(E_j - E'_j). \quad (\text{B.3})$$

Damping constants  $\gamma_j$ ,  $\gamma_j = \pi|V_j|^2$ , and shifted energies  $\tilde{E}_j^0$ ,  $\tilde{E}_j^0 = E_j^0 + \mathcal{P} \int dE |V_j(E)|^2 / (E_j^0 - E)$ , have been introduced in Eq. (B.3). Symbol  $\epsilon$  denotes a small positive number and limit  $\epsilon \rightarrow 0$  is assumed at the end of calculations.

After the transformations, Hamiltonians  $H_j^L$  defined in Eq. (3) attain the form:

$$\hat{H}_j^L = \int dE_j \bar{\mu}_j(E_j) \alpha_L \exp(-iE_L t) |E_j\rangle_j \langle 0| + \text{H.c.} \quad (\text{B.4})$$

Dipole moments  $\bar{\mu}_j(E_j)$  describing excitation/ionization of states  $|E_j\rangle$  inside the structured continua are derived in the form

$$\bar{\mu}_j(E_j) = \tilde{\mu}_j \frac{\epsilon_j(E_j) + q_j}{\epsilon_j(E_j) - i}; \quad (\text{B.5})$$

$\epsilon_j(E) = (E - \tilde{E}_j^0) / \gamma_j$ ,  $q_j = \mu_j / (\pi \tilde{\mu}_j V_j^*)$ , and  $i$  stands for the imaginary unit. If the dipole-dipole interaction between two atoms is neglected, we have  $\bar{\mu}_a(E_a^F) = \bar{\mu}_b(E_b^F) = 0$  for  $E_a^F - \tilde{E}_a^0 = -\gamma_a q_a$  and  $E_b^F - \tilde{E}_b^0 = -\gamma_b q_b$ . Thus, there occurs one Fano zero with energy  $E_a^F$  in the photoelectron ionization spectrum of atom  $a$  and one Fano zero with energy  $E_b^F$  in the spectrum of atom  $b$ .

These Fano zeros are concealed by the dipole-dipole interaction. The greatest competition of two parts of the dipole-dipole interaction is observed provided that the matrix element of transfer Hamiltonian  $\hat{H}_{\text{trans}}$  between states  $|E_a^F\rangle$  and  $|E_b^F\rangle$  equals zero. Hamiltonian  $\hat{H}_{\text{trans}}$  given in Eq. (4) is expressed in these bases as

$$\hat{H}_{\text{trans}} = \int dE_a \int dE_b \bar{J}(E_a, E_b) |E_b\rangle \langle E_a| + \text{H.c.}, \quad (\text{B.6})$$

where

$$\begin{aligned} \bar{J}(E_a, E_b) &= J_{ab} f_a(E_a) f_b^*(E_b) \\ &+ \int dE'_a J_a^* g_a(E_a, E'_a) f_b^*(E_b) \\ &+ \int dE'_b J_b f_a(E_a) g_b^*(E_b, E'_b). \end{aligned} \quad (\text{B.7})$$

The use of expressions written in Eqs. (B.3) transforms equation (B.7) into the form:

$$\begin{aligned} \bar{J}(E_a, E_b) &= \frac{J_a^* V_b}{\gamma_b [\epsilon_b(E_b) - i]} + \frac{J_b V_a^*}{\gamma_a [\epsilon_a(E_a) + i]} \\ &+ \frac{J_{ab} V_a^* V_b - i J_a^* V_b \gamma_a + i J_b V_a^* \gamma_b}{\gamma_a \gamma_b [\epsilon_a(E_a) + i] [\epsilon_b(E_b) - i]}. \end{aligned} \quad (\text{B.8})$$

The requirement  $\bar{J}(E_a^F, E_b^F) = 0$  results in the following condition for the values of dipole-dipole interaction constants  $J_{ab}$ ,  $J_a$  and  $J_b$ :

$$\frac{J_a^* \mu_a^*}{\tilde{\mu}_a^*} + \frac{J_b \mu_b}{\tilde{\mu}_b} = J_{ab}. \quad (\text{B.9})$$

Assuming identical atoms  $a$  and  $b$  and real interaction constants, the condition in Eq. (B.9) simplifies

$$\frac{J_a}{J_{ab}/2} = \frac{\tilde{\mu}_a}{\mu_a}. \quad (\text{B.10})$$

## References

- [1] L. Journal, B. Rouvellou, D. Cubaynes, J. M. Bizau, F. J. Willeumier, M. Richter, P. Sladeczek, K.-H. Selbman, P. Zimmerman, and H. Bergerow. First observation of a Fano profile following one step autoionization into a double photoionization continuum. *J. de Physique IV*, 3:217–226, 1993.
- [2] Ph. Durand, I. Paidarová, and F. X. Gadéa. Theory of Fano profiles. *J. Phys. B: At. Mol. Opt. Phys.*, 34:1953–1966, 2001.
- [3] G. S. Agarwal, S. L. Haan, and J. Cooper. Quantum anti-Zeno effect. *Phys. Rev. A*, 29:2552–2565, 1984.
- [4] W. Leoński, R. Tanaś, and S. Kielich. Laser-induced autoionization from a double Fano system. *J. Opt. Soc. Am. B*, 4:72–77, 1987.
- [5] W. Leoński and R. Tanaś. Dc-field effects on the photoelectron spectrum from a system with two autoionising levels. *J. Phys. B: At. Mol. Opt. Phys.*, 21:2835–2844, 1988.
- [6] W. Leoński, R. Tanaś, and S. Kielich. Effect of dc field coupling on the photoelectron spectrum from double auto-ionising levels. *J. Phys. D: Appl. Phys.*, 21:S125, 1988.
- [7] T. Aberg. Asymptotic double-photoexcitation cross sections of the Helium atom. *Phys. Rev. A*, 2:1726–1729, 1970.
- [8] F. W. Byron Jr. and C. J. Joachain. Correlation effects in atoms. II. angular correlations between electrons. *Phys. Rev.*, 157:1–6, 1967.
- [9] M. Wickenhauser, J. Burgdörfer, F. Krausz, and M. Drescher. Time resolved Fano resonances. *Phys. Rev. Lett.*, 94:023002, 2005.
- [10] Z. X. Zhao and C. D. Lin. Theory of laser-assisted autoionization by attosecond light pulses. *Phys. Rev. A*, 71:060702(R), 2005.
- [11] X. M. Tong and C. D. Lin. Double photoexcitation of He atoms by attosecond xuv pulses in the presence of intense few-cycle infrared lasers. *Phys. Rev. A*, 71:033405, 2005.
- [12] P. Eckle, M. Smolarski, P. Schlup, J. Biegert, A. Staudte, M. Schöffler, H. G. Muller, R. Dörner, and U. Keller. Attosecond angular streaking. *Nat. Phys.*, 41:565–570, 2008.
- [13] S. Gilbertson, M. Chini, X. Feng, S. Khan, Y. Wu, and Z. Chang. Monitoring and controlling the electron dynamics in Helium with isolated attosecond pulses. *Phys. Rev. Lett.*, 105:263003, 2010.
- [14] U. Fano. Effects of configuration interaction on intensities and phase shifts. *Phys. Rev.*, 124:1866–1878, 1961.
- [15] P. Lambropoulos and P. Zoller. Autoionizing states in strong laser fields. *Phys. Rev. A*, 24:379–397, 1981.
- [16] K. Rzażewski and J. H. Eberly. Confluence of bound-free coherences in laser-induced autoionization. *Phys. Rev. Lett.*, 47:408–412, 1981.
- [17] M. Lewenstein, J. W. Haus, and K. Rzażewski. Photon spectrum in laser-induced autoionization. *Phys. Rev. Lett.*, 50:417, 1983.

- [18] A. Palacios, J. Feist, A. González-Castrillo, J. L. Sanz-Vicario, and F. Martín. Autoionization of molecular hydrogen: Where do the Fano lineshapes Go? *ChemPhysChem*, 14:1456–1463, 2013.
- [19] S. J. van Enk, J. Zhang, and P. Lambropoulos. Pump-induced transparency and enhanced third-harmonic generation near an autoionizing state. *Phys. Rev. A*, 50:3362–3365, 1994.
- [20] A. Raczynski, M. Rzepecka, J. Zaremba, and S. Ziełńska-Kaniasty. Electromagnetically induced transparency and light slowdown for  $\lambda$ -like systems with a structures continuum. *Optics Communications*, 266:552–557, 2006.
- [21] T. B. Dinh, V. Cao Long, W. Leoński, and J. Peřina Jr. Electromagnetically induced transparency for a double Fano-profile system. *Eur. Phys. J. D*, 68:150, 2014.
- [22] A. Raczynski and J. Zaremba. Threshold effects in photoionization and photodetachment. *Phys. Rep.*, 235:1–55, 1993.
- [23] M. Lewenstein and K. Rzażewski. Quantum anti-Zeno effect. *Phys. Rev. A*, 61:022105, 2000.
- [24] K. Rzażewski and J. H. Eberly. Photoexcitation of an autoionizing resonance in the presence of off-diagonal relaxation. *Phys. Rev. A*, 27:2026, 1983.
- [25] W. Leoński and V. Bužek. Quantum laser field effect on the photoelectron spectrum for auto-ionizing systems. *J. Mod. Opt.*, 37:1923–1934, 1990.
- [26] W. Leoński. Squeezed-state effect on bound-continuum transitions. *J. Opt. Soc. Am. B*, 10:244–252, 1993.
- [27] A. Ridolfo, O. Di Stefano, N. Fina, R. Saija, and S. Savasta. Quantum plasmonics with quantum dot-metal nanoparticle molecules: Influence of the Fano effect on photon statistics. *Phys. Rev. Lett.*, 105:263601, 2010.
- [28] V. Giannini, Y. Francescato, H. Amrania, C. C. Phillips, and S. A. Maier. Fano resonances in nanoscale plasmonic systems: A parameter-free modeling approach. *Nano Letters*, 11:2835–2840, 2011.
- [29] A. E. Miroshnichenko, S. Flach, and Y. S. Kivshar. Fano resonances in nanoscale structures. *Rev. Mod. Phys.*, 82:2257, 2010.
- [30] L. Karwacki, P. Trocha, and J. Barnas. Spin-dependent thermoelectric properties of a Kondo-correlated quantum dot with Rashba spin-orbit coupling. *J. Phys.-Cond. Matt.*, 25, 2013.
- [31] V. A. Fedotov, A. Tsiatmas, J. H. Shi, R. Buckingham, P. de Groot, Y. Chen, S. Wang, and N. I. Zheludev. Temperature control of Fano resonances and transmission in superconducting metamaterials. *Opt. Express*, 18(9):9015–9019, 2010.
- [32] M. Fogelström, M. J. Graf, V. A. Sidorov, X. Lu, E. D. Bauer, and J. D. Thompson. Two-channel point-contact tunneling theory of superconductors. *Phys. Rev. B*, 90:104512, 2014.
- [33] R. Szczesniak and A. P. Durajski. The energy gap in the  $(\text{Hg}_{1-x}\text{Sn}_x)\text{Ba}_2\text{Ca}_2\text{Cu}_3\text{O}_{8+y}$  superconductor. *J. Supercond. Nov. Magn.*, 27:1363–1367, 2014.
- [34] H. Feshbach. A unified theory of nuclear reactions. II. *Ann. Phys.*, 19:287–313, 1962.
- [35] S. Inouye, M. R. Andrews, J. Stenger, H.-J. Miesner, D. M. Stamper-Kurn, and W. Ketterle. Observation of Feshbach resonances in a Bose-Einstein condensate. *Nature*, 392:151–154, 1994.
- [36] L. S. Cederbaum, J. Zobeley, and F. Taran. Giant intermolecular decay and fragmentation of clusters. *Phys. Rev. Lett.*, 79:4778–4781, 1997.
- [37] B. Najjari, A. B. Voitkiv, and C. Müller. Two-center resonant photoionization. *Phys. Rev. Lett.*, 105:153002, 2010.
- [38] A. B. Voitkiv and B. Najjari. Two-center dielectronic recombination and resonant photoionization. *Phys. Rev. A*, 82:052708, 2010.
- [39] C. Müller, A. B. Voitkiv, J. R. Crespo López-Urrutia, and Z. Harman. Strongly enhanced recombination via two-center electronic correlations. *Phys. Rev. Lett.*, 104:233202, 2010.
- [40] V. Averbukh, U. Saalman, and J. M. Rost. Suppression of exponential electronic decay in a charged environment. *Phys. Rev. Lett.*, 104:233002, 2010.
- [41] B. Walker, B. Sheehy, L. F. DiMauro, P. Agostini, K. J. Schafer, and K. C. Kulander. Precision measurement of strong field double ionization of Helium. *Phys. Rev. Lett.*, 73:1227–1230, 1994.
- [42] T. Weber, H. Giessen, M. Weckenbrock, G. Urbasch, A. Staudte, L. Spielberger, O. Jagutzki, V. Mergel, M. Vollmer, and R. Dörner. Correlated electron emission in multiphoton double ionization. *Nature*, 405:658–661, 2000.
- [43] A. Rudenko, V. L. B. de Jesus, T. Ergler, K. Zrost, B. Feuerstein, C. D. Schröter, R. Moshhammer, and J. Ullrich. Correlated two-electron momentum spectra for strong-field nonsequential double ionization of He at 800 nm. *Phys. Rev. Lett.*, 99:263003, 2007.
- [44] T. Morishita, S. Watanabe, and C. D. Lin. Attosecond light pulses for probing two-electron dynamics of Helium in the time domain. *Phys. Rev. Lett.*, 98:083003, 2007.
- [45] M. Uiberacker, T. Uphues, M. Schultze, A. J. Verhoef, V. Yakovlev, M. F. Kling, J. Rauschenberger, N. M. Kabachnik, H. Schröder, M. Lezius, K. L. Kompa, H.-G. Muller, M. J. J. Vrakking, S. Hendel, U. Kleineberg, U. Heinzmann, M. Drescher, and F. Krausz. Attosecond real-time observation of electron tunnelling in atoms. *Nature*, 446:627–632, 2007.
- [46] J. Peřina Jr., A. Lukš, W. Leoński, and V. Peřinová. Photoelectron spectra in an autoionization system interacting with a neighboring atom. *Phys. Rev. A*, 83:053430, 2011.
- [47] J. Peřina Jr., A. Lukš, W. Leoński, and V. Peřinová. Photoionization electron spectra in a system interacting with a neighboring atom. *Phys. Rev. A*, 83:053416, 2011.
- [48] A. Lukš, J. Peřina Jr., W. Leoński, and V. Peřinová. Entanglement between an autoionizing system and a neighboring atom. *Phys. Rev. A*, 85:012321, 2012.
- [49] V. Peřinová, A. Lukš, J. Křepelka, and J. Peřina Jr. Quantum correlation and entanglement between an ionizing system and a neighboring atom interacting directly and via a quantized field. *Phys. Rev. A*, 90:033428, 2014.
- [50] S. Hill and W. K. Wootters. Computable entanglement. *Phys. Rev. Lett.*, 78:5022, 1997.
- [51] A. Peres. Separability criterion for density matrices. *Phys. Rev. Lett.*, 77:1413–1415, 1996.
- [52] M. Horodecki, P. Horodecki, and R. Horodecki. Separability of mixed states: Necessary and sufficient conditions. *Phys. Lett. A*, 223:1–8, 1996.
- [53] J. Peřina Jr., A. Lukš, V. Peřinová, and W. Leoński. Photoelectron ionization spectra in a system interacting with a neighbor atom. *J. Russian Laser Res.*, 32:454–466, 2011.
- [54] J. Peřina Jr., A. Lukš, V. Peřinová, and W. Leoński. Fano zeros in photoelectron spectra of an autoionization system interacting with a neighboring atom. *Opt. Express*, 19:17133–17142, 2011.
- [55] Z. Ficek. Quantum entanglement and disentanglement of multi-atom systems. *Front. Phys. China*, 5:26–81, 2010.
- [56] E. A. Silinsh and V. Čápek. *Organic Molecular Crystals: Interaction, Localization and Transport Phenomena*. Oxford University Press/American Institute of Physics, 1994.
- [57] P. Meystre and P. Sargent III. *Elements of Quantum Optics*. Springer, Berlin, 2007.

- [58] S. H. Autler and C. H. Townes. Stark effect in rapidly varying fields. Phys. Rev., 100:703–722, 1955.